Measurement of Magneto-Optical Kerr Effect Using Piezo-Birefringent Modulator

JAPANESE JOURNAL OF APPLIED PHYSICS
VOL. 20, NO. 12, DECEMBER, 1981 pp. 2403–2409

Measurement of Magneto-Optical Kerr Effect Using Piezo-Birefringent Modulator

Katsuaki SATO

Broadcasting Science Research Laboratories of Nippon Hoso Kyokai, 1–10–11 Kinuta, Setagaya-ku, Tokyo 157

(Received July 11, 1981; accepted for publication September 19, 1981)

An advanced magneto-optical technique is described, which allows simultaneous determination of two mutually-conjugate parameters—Kerr rotation and reflectance magneto-circular dichroism—using a piezo-birefringent modulator. This technique provides a sensitivity of 0.002° for Kerr rotation at $\lambda=500$ nm with 12 nm resolution, using a halogen lamp (150 W) as the light source. The wavelength region covered by the method can be extended from 300–2500 nm by suitable selection of gratings and light detectors. The new technique was used to measure magneto-optical hysteresis loops for several wavelengths and magneto-optical spectra on an rf-sputtered amorphous Gd–Co film, and the results are reported here.

§1. Introduction

There are various techniques in use for measuring the magneto-optical Kerr effect. The polarization modulation method using a Faraday cell[1] is known to give high sensitivity ($\sim$0.001° at 500 nm), but this method is affected by stray magnetic fields and is limited in its wavelength span. In addition, continuous recording is difficult except with sophisticated electronics. The spinning analyzer technique[2] is superior to the Faraday cell method, since it is insensitive to stray fields, is limited in wavelength only by the characteristics of the polarizing element, and can be used for continuous recording. However, the sensitivity is rather poor ($\sim$0.01° at 700 nm) because of jitter in the rotation mechanism. Another disadvantage of these methods is that measurement of Kerr ellipticity requires the insertion of a quarter-wave plate in the optical path; an appropriate quarter-wave plate should be selected for each wavelength region of measurement, which imposes another problem on continuous recording.

In the past few years a number of experiments have been carried out using piezo-birefringent modulators for ellipsometry and measurements of magneto-circular dichroism.[3–6] The author has recently developed an apparatus for continuous recording of magneto-optical spectra using a piezo-birefringent modulator. This apparatus provides a sensitive method for the simultaneous determination of two magneto-optical parameters—Kerr rotation ϕ_K and reflectance magneto-circular dichroism (RMCD) $\Delta R/R$.*

Apart from the introduction, this paper consists of four sections; §2 presents the principles of the technique; §3, the methods of calibration; §4, details of the newly-designed system; and §5, some results of magneto-optical measurements on an amorphous Gd–Co film using the apparatus.

§2. Principles of the Technique

A schematic diagram showing the principle of the method is given in Fig. 1. The coordinates are taken as shown in the figure; the z-axis is parallel to the direction of propagation of the incident light, the y-axis is located in the plane of incidence, and the x-axis is perpendicular to the zy-plane.

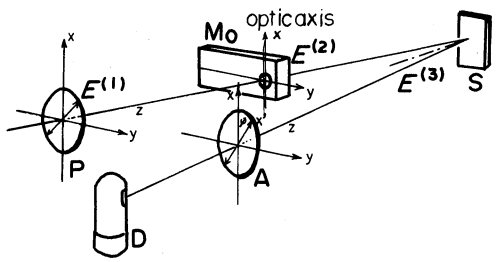

Fig. 1. Schematic diagram showing essentials of the measuring technique. P: polarizer, Mo: modulator, A: analyzer, D: detector. The polarizing angle of P makes an angle 45° with the x-axis. The polarizing angle of A is assumed to be ϕ.

*RMCD can be related to Kerr ellipticity η_K by the simple relation of eq. (4).

Since the near-normal incidence condition holds in our system, the same coordinates are assumed for the reflected beam; the reflected light propagates in the $-z$ direction.

In Fig. 1, P denotes the polarizer, the polarizing axis of which makes an angle of 45° with the x-axis, and Mo denotes the piezo-birefringent modulator, the optical axis of which is in the x-direction. The light passing through Mo receives a periodically-varying retardation δ which is described by

$$\delta=\delta_0 \sin 2\pi pt, \tag{1}$$

where δ_0 denotes the amplitude of the retardation and p the modulation frequency.

Modulated light is reflected by a sample S. For simplicity, it is assumed that the sample is optically isotropic in the absence of a magnetic field. As described before, we assume that the angle of incidence is small enough to ensure the near-normal incidence condition, under which the reflection of light is described in terms of the Fresnel coefficients $\hat{r}_{\pm}$, where $\hat{r}_+=r_+ e^{i\theta_+}$ and $\hat{r}_-=r_- e^{i\theta_-}$ for RCP (right-circularly polarized light) and LCP (left-circularly polarized light), respectively. Here it is assumed that the equations $r_+=r_-$ and $\theta_+=\theta_-$ hold when macroscopic magnetization of the sample is absent. The reflected light passes through an analyzer A, the polarizing axis of which is along the x'-axis, which makes an angle ϕ with the x-axis. The insertion of the analyzer is essential to the present technique. Finally, the light is detected by a photodetector D, either a photomultiplier or an InSb photocell.

In the following analysis, we neglect the effects of reflection and absorption by the optical elements employed. Neglect of these effects is probably not serious, because the final results are always in the form of the ratio of the modulated component to the dc component of the detected light, as will be shown in eqs. (13) and (14). In addition, the calibration processes given in §3 will remove any remaining influences.

Given that E denotes the amplitude of the electric field vector $\boldsymbol{E}^{(1)}$ of the light transmitted through P, the amplitude $E_{x'}$ of the light transmitted from A can be described as follows:

$$E_{x'}=\frac{E}{2\sqrt{2}}\{\hat{r}_+(1-i\,e^{i\delta})\,e^{i\phi}+\hat{r}_-(1+i\,e^{i\delta})\,e^{-i\phi}\}, \tag{2}$$

as derived in the Appendix.

The intensity I of the light detected by D, which is expressed by $\varepsilon/4\pi\cdot|E_{x'}|^2$, is given by

$$I=\frac{\varepsilon E^2}{16\pi}\left\{R+\frac{\Delta R}{2}\sin\delta+R\sin(\Delta\theta+2\phi)\cos\delta\right\}, \tag{3}$$

where R, ΔR and $\Delta\theta$ are defined as

$$R=\frac{1}{2}(r_+^2+r_-^2),\quad \Delta R=r_+^2-r_-^2,$$

and

$$\Delta\theta=\theta_+-\theta_-.$$

In the derivation of eq. (3), the condition $\Delta R/R\ll 1$ has been employed.

The magneto-optical parameters—Kerr rotation ϕ_K and Kerr ellipticity η_K—can be expressed in terms of $\Delta\theta$ and $\Delta R/R$ by the following equations:

$$\phi_K=-\frac{1}{2}\Delta\theta,\quad \eta_K=\frac{1}{4}(\Delta R/R). \tag{4}$$

By applying eq. (1) to eq. (3) and by using the expansion formulae

$$\sin(\delta_0\sin 2\pi pt)=2J_1(\delta_0)\sin 2\pi pt+\cdots,$$

$$\cos(\delta_0\sin 2\pi pt)=J_0(\delta_0)+2J_2(\delta_0)\sin 4\pi pt+\cdots, \tag{5}$$

where $J_n(x)$ is an n-th order Bessel function, we obtain

$$I=I(0)+I(p)\sin 2\pi pt+I(2p)\sin 4\pi pt+\cdots, \tag{6}$$

in which

$$I(0)=I_0R\{1+J_0(\delta_0)\sin(\Delta\theta+2\phi)\}, \tag{7}$$

$$I(p)=I_0\Delta RJ_1(\delta_0), \tag{8}$$

$$I(2p)=2I_0RJ_2(\delta_0)\sin(\Delta\theta+2\phi). \tag{9}$$

In these equations I_0 represents $(\varepsilon/8\pi)E^2$.

The output voltage of the detector D therefore consists of three components; a dc component, a p-component and a $2p$ component. If the sensitivities of the detection-amplification systems for the dc, p and $2p$ components are given by q_1, q_2 and q_3, respectively, we obtain the intensities I_1 for dc, I_2 for p and I_3 for $2p$ components as follows:

$$I_1=q_1I_0R\{1+J_0(\delta_0)\sin(\Delta\theta+2\phi)\}, \tag{10}$$

$$I_2=q_2I_0\Delta RJ_1(\delta_0), \tag{11}$$

$$I_3=2q_3I_0RJ_2(\delta_0)\sin(\Delta\theta+2\phi). \tag{12}$$

The ratios I_2/I_1 and I_3/I_1 are then given by

$$\frac{I_2}{I_1}=A\frac{J_1(\delta_0)\Delta R/R}{1+J_0(\delta_0)\sin(\Delta\theta+2\phi)}, \tag{13}$$

$$\frac{I_3}{I_1}=B\frac{2J_2(\delta_0)\sin(\Delta\theta+2\phi)}{1+J_0(\delta_0)\sin(\Delta\theta+2\phi)}, \tag{14}$$

where $A=q_2/q_1$ and $B=q_3/q_1$.

These equations give simple results in the following two cases:

Case I. $\phi=0$

Since the phase shift $\Delta\theta$ is considered to be much smaller than unity, eqs. (13) and (14) can be approximated by

$$\frac{I_2}{I_1}=AJ_1(\delta_0)\frac{\Delta R}{R}, \tag{15}$$

$$\frac{I_3}{I_1}=BJ_2(\delta_0)2\Delta\theta. \tag{16}$$

The coefficients A and B can be determined by the calibration procedure described in §3.

Therefore, we are able to calculate the values of the magneto-optical parameters $\Delta R/R$ and $\Delta\theta$ from experimental values of I_2/I_1 and I_3/I_1 by using the simple relations (15) and (16).

Case II. $\Delta\theta=-2\phi$

In this case, $\sin(\Delta\theta+2\phi)$ in eqs. (13) and (14) vanishes, thus giving $I_3/I_1=0$. Therefore, we can determine $\frac{1}{2}\Delta\theta(=-\phi_K)$ by accurate measurement of the angle ϕ where I_3 vanishes. $\Delta R/R$ cannot be determined in this case.

Figure 2 shows a schematic explanation of why the p and $2p$ components of the detected signal represent RMCD and Kerr rotation, respectively.

Curve (a) shows the time dependence of the retardation produced by the modulator Mo. The amplitude δ_0 of a retardation δ is taken as $\pi/2$ in the figure for simplicity of illustration; in this case, the maximum and minimum of δ correspond to circularly-polarized light. Provided that the sample S causes neither rotation nor circular dichroism, the vector loci of the electric field $E^{(3)}$ can be illustrated as (b); the variation is LP-RCP-LP-LCP-LP in one period of modulation, where LP denotes linear polarization. The projection of $E^{(3)}$ onto the horizontal (x) axis is constant against time, as shown in (c).

When a difference between phase shifts for RCP and LCP, i.e., Kerr rotation, exists, the plane of the linearly-polarized light rotates, producing a change in the x-projection of $E^{(3)}$, while the vector loci for circularly-polarized light remain unchanged. Thus a $2p$ component appears in the x-projection as seen in (e).

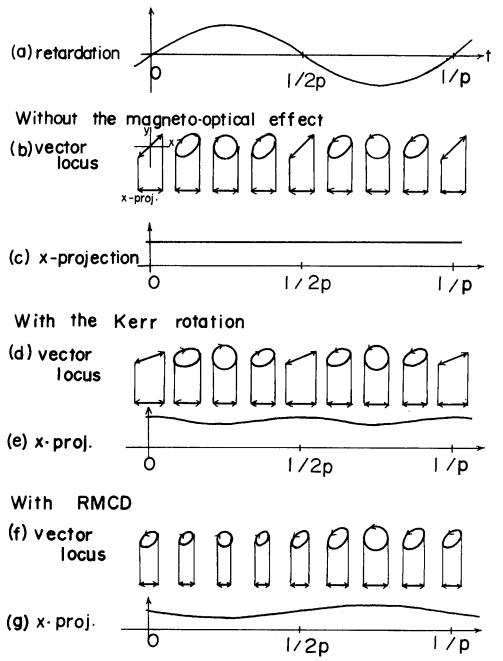

Fig. 2. Schematic illustration of why the pHz and the $2p$Hz components represent RMCD and Kerr rotation, respectively.

On the other hand, when RMCD is present, the vector lengths for RCP and LCP become different as illustrated in (f), resulting in the appearance of a p component in the x-projection (g).

In this way, we can measure Kerr rotation and RMCD by detecting the p and the $2p$ components, respectively.

§3. Calibration

3.1 *Calibration of the Kerr rotation angle*

The Kerr rotation angle can be calibrated if we can estimate the value of $BJ_2(\delta_0)$ in eq. (16).

For this purpose, we replace the sample S by a plane mirror of aluminum or silver and set the polarizing angle ϕ of the analyzer A at $\pm\pi/4$. We can assume that the relations $\Delta R=0$ and $\Delta\theta=0$ hold for the plane mirror. Then we get from eq. (14)

$$\frac{I_3}{I_1}=\pm\frac{2BJ_2(\delta_0)}{1\pm J_0(\delta_0)}, \tag{17}$$

where the double sign corresponds to $\phi = \pm\pi/4$.

We can determine $J_0(\delta_0)$ by taking the ratio of $(I_3/I_1)_{\phi=\pi/4}$ to $(I_3/I_1)_{\phi=-\pi/4}$. Using eq. (17) and the value of $J_0(\delta_0)$ thus determined, we can obtain the value of $2BJ_2(\delta_0)$.

3.2 *Calibration of RMCD*

$\Delta R/R$ can be calibrated if we can estimate the value of $AJ_1(\delta_0)$ in eq. (15). For this purpose, we replace the sample S by a plane mirror and set the polarizing angle of the analyzer A at $\pm\pi/4$, as was done in §3.1. In addition, we insert a quarter-wave plate in the optical path between the modulator and the plane mirror. Under these conditions, we have from eq. (3)

$$I = \frac{1}{2} I_0 R(1 \pm \cos\delta), \tag{18}$$

in which we assume that both ΔR and $\Delta\theta$ of the plane mirror can be neglected under the near-normal incidence condition.

The retardation δ in this case should contain that of the quarter-wave plate in addition to that caused by the modulator; thus giving

$$\delta = \delta_\lambda + \delta_0 \sin 2\pi pt, \tag{19}$$

where $\delta_\lambda = (\pi/2)(\lambda/\lambda_0)$, λ_0 being the wavelength at which the retardation of the quarter-wave plate has the value $\pi/2$.

By putting eq. (19) into eq. (18) and using eq. (5) we obtain

$$I = \frac{1}{2} I_0 R\{1 \pm J_0(\delta_0)\cos\delta_\lambda \mp 2J_1(\delta_0)\sin\delta_\lambda \sin 2\pi pt \pm 2J_2(\delta_0)\cos\delta_\lambda \sin 4\pi pt\}. \tag{20}$$

From this equation we get, instead of eqs. (10) and (11),

$$I_1 = \frac{1}{2} q_1 I_0 R\{1 \pm J_0(\delta_0)\cos\delta_\lambda\}, \tag{21}$$

$$I_2 = \mp q_2 I_0 R J_1(\delta_0)\sin\delta_\lambda \sin 2\pi pt. \tag{22}$$

Hence

$$\frac{I_2}{I_1} = \mp \frac{2AJ_1(\delta_0)}{1 \pm J_0(\delta_0)\cos\delta_\lambda}, \tag{23}$$

where $A = q_2/q_1$ and the double sign corresponds to $\phi = \pm\pi/4$.

If the wavelength λ is equal to λ_0, $\cos\delta_\lambda$ vanishes, so eq. (23) becomes

$$\frac{I_2}{I_1} = \mp 2AJ_1(\delta_0), \tag{24}$$

by which we can calibrate the coefficient $AJ_1(\delta_0)$ in eq. (15).

§4. Details of the System

4.1 *Optical layouts*

This section describes the way in which the apparatus is set up for measuring the reflectance magneto-optical spectrum, using the principles developed in the preceding sections.

Figure 3 is a schematic diagram of the total system. In this figure, L is the light source (150 W halogen-tungsten lamp), Mc the mono-

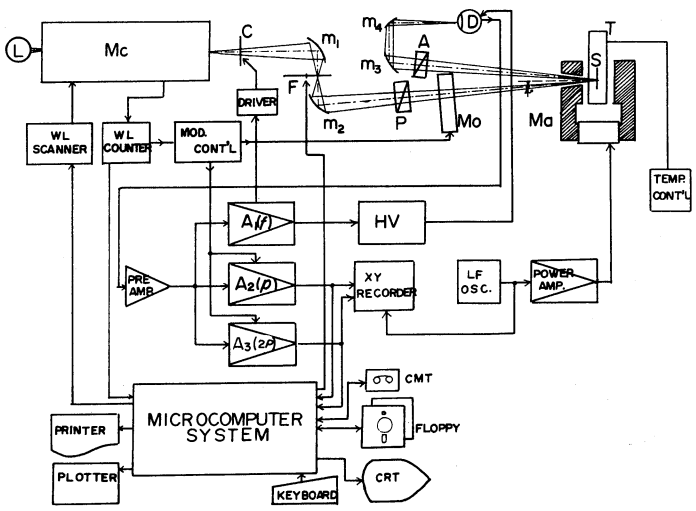

Fig. 3. Overall block diagram of our system. For symbols see text.

chromator (Nikon P250 equipped with gratings with blaze wavelengths of 300 nm, 750 nm and 2000 nm), C a rotating light-chopper (frequency $f \sim 330$ Hz), F a filter mounted on an exchangeable filter-selector, m_1 and m_2 off-axis ellipsoidal mirrors, P and A Gran prism polarizers with 20 mm ϕ aperture (Halle Inc.), Mo a piezo-birefringent modulator of modulation frequency 50 kHz (Morvue Inc. Photoelastic Modulator PEM-CF3), m_3 a plane mirror, m_4 a spherical mirror, and D a detector—a photomultiplier (Hamamatsu R636) for wavelengths between 300 and 900 nm or a liquid-nitrogen-cooled InSb photocell (Hamamatsu P839S) for 900–2500 nm.

A sample S is placed in the cryostat T. The sample temperature can be varied from -25°C to 70°C by using a Peltier-thermomodule (Komatsu-Marlow MI-1142). The magnetic field is applied perpendicular to the sample surface, which provides a polar Kerr-effect condition. For magnetic fields of less than 1.5 kOe, a small electromagnet with a window in its pole piece is employed. If we need higher fields or lower temperatures, we use a superconducting solenoid with a variable-temperature insert (Oxford SM-4), thus obtaining a magnetic field up to 50 kOe and a temperature between 2 K and 300 K.

The light from Mc is focused by m_1 and m_2 onto the sample surface. The retardation of the light is modulated at 50 kHz by Mo before being reflected by the sample S. The amplitude δ_0 of the modulated retardation is kept constant ($\pi/2$) over the whole wavelength region, by supplying a wavelength-proportional voltage to the input of the modulator-controller. This voltage is supplied by a D/A converter from the digital output of the wavelength counter attached to the monochromator.

The angle of incidence to the sample surface is 4°, which is near-normal incidence. The reflected beam passes through A and is focused on D by m_3 and m_4. The detector often picks up a spurious p signal radiated from the nearby modulator, which amounts to as much as ten times the true signal. To avoid this problem, a light guide is employed, making it possible to separate the photo-detector from the modulator.

4.2 *Electronics*

The output signal of D is fed to a preamplifier, where the current output is converted into a voltage signal. The preamplifier output feeds three lock-in amplifiers A_1, A_2 and A_3, which amplify the f, p and $2p$ components, respectively. The f component, which is synchronous with the chopping frequency of the chopper C, corresponds to the dc output I_1 given in eq. (10), and the p and $2p$ components to I_2 and I_3 given in eqs. (11) and (12), respectively. The lock-in amplifiers used are LI473 and LI573 (NF Circuit Design Block Inc.) for A_1 and A_2 and a PAR model 124A for A_3.

The ratios I_2/I_1 for RMCD and I_3/I_1 for Kerr rotation can be calculated by a combination of a feedback technique which keeps I_1 nearly constant and a microcomputer technique. To keep I_1 constant, I_1 is fed back to a high-voltage supply for a photomultiplier or to a power supply for a light source.

Automatic repetition measurements of magneto-optical spectra are performed with the aid of a microprocessor-based data-acquisition system. Data are stored on a floppy-disk file and are processed by the same system. The results are plotted by a curve plotter.

The sensitivity of Kerr rotation is less than 0.002° at 500 nm with a resolution of 12 nm using a 150 W halogen lamp as the light source. Higher sensitivity has been obtained by data processing of "repeated" measurements using the microcomputer.

Magneto-optical hysteresis loops can be obtained by sweeping the current of the electromagnet, driving a power amplifier with a slowly-varying triangular-wave voltage.

§5. Example—Magneto-optical Effects of a Sputtered Amorphous Gd–Co Film

Amorphous Gd–Co films have been attracting attention for possible use as thermomagnetic recording media.[7] There have been only a few reports on the magneto-optical spectra of the film,[8,9] referring only to one or other of the two magneto-optical parameters.

The author has recently measured both the Kerr rotation and the RMCD of a film using the newly-designed apparatus described in the previous sections. In this section, some of the results are presented as an example of data obtained by the technique.

Figure 4 shows the wavelength dependence of magneto-optical hysteresis loops of an rf-sputtered amorphous Gd–Co film measured from the substrate side (through the glass) at −25°C. The solid and dotted curves represent Kerr rotation and RMCD, respectively.

Kerr rotation loops for short wavelengths show a field-proportional component, which is caused by the Faraday rotation of both the substrate and the window material of the cryostat. This effect is less evident for longer wavelengths ($\lambda > 800$ nm). In the RMCD loops, on the other hand, the field-proportional term is negligible, since magneto-circular dichroism of glass is very small for the transparent wavelengths.

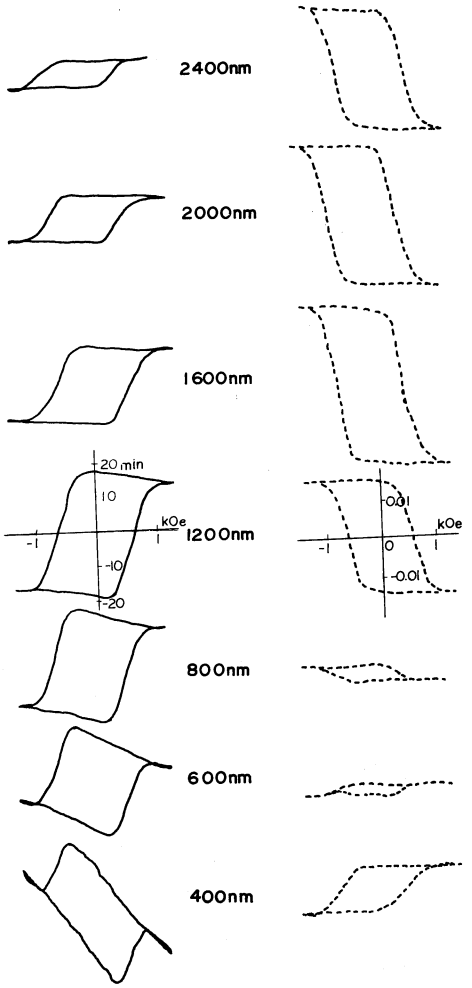

Fig. 4. Magneto-optical hysteresis loops of rf-sputtered amorphous Gd–Co film for several wavelengths. Solid curve represents Kerr rotation and dotted one RMCD.

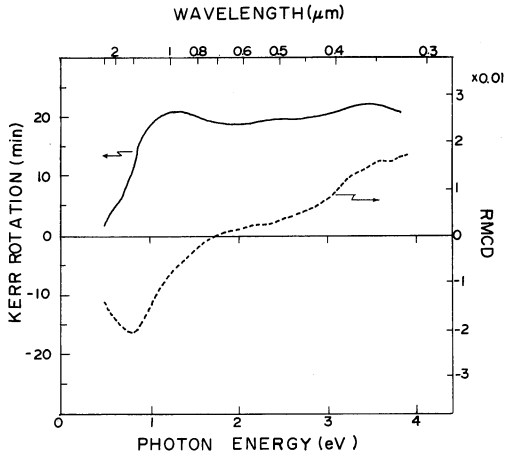

Fig. 5. Magneto-optical spectra of rf-sputtered amorphous Gd–Co film. Solid curve represents Kerr rotation and dotted one RMCD.

The Kerr rotation spectrum and RMCD spectrum are given in Fig. 5 for the same film as in Fig. 4. To avoid the Faraday effect of the substrate and the window, measurements were performed at remanence magnetization; after applying a plus or minus magnetic field sufficient to saturate the sample, the field was decreased to zero. As mentioned in the previous section, the difference between the plus zero data and the minus zero data was calculated.

From Figs. 4 and 5, it can be seen that our Gd–Co film shows only a slight spectral variation of ϕ_K in the 0.3–1.2 μm wavelength region; a small peak is observed at about 1 μm. This fact favors the use of near-ir semiconductor lasers instead of the He–Ne laser conventionally used for magneto-optical readout. On the other hand, the RMCD spectrum shows a prominent structure; the value decreases as the wavelength is increased and changes sign, and has an extremum value at around 1.5 μm. The wavelength where the RMCD changes sign varies from sample to sample depending on the preparation conditions of the film. The effect on the magneto-optical properties of the application of a negative dc bias and the introduction of oxygen during the film preparation is now under investigation.

Acknowledgements

The author would like to express his thanks to Dr. T. Teranishi for useful discussions, to Mr. Y. Togami for supplying the Gd–Co films used in this study, and to Mr. T. Ando for his

help in the measurement of the magneto-optical spectra.

Appendix

In Fig. 1, the electric field vector $\boldsymbol{E}^{(1)}$, which is transmitted through the polarizer P is expressed by

$$\boldsymbol{E}^{(1)}=\frac{E}{\sqrt{2}}\boldsymbol{i}+\frac{E}{\sqrt{2}}\boldsymbol{j}, \qquad (A\cdot 1)$$

where the polarizing axis of P is assumed to make an angle of $\pi/4$ with the x-axis, and $\boldsymbol{i}$ and $\boldsymbol{j}$ denote unit vectors for the x and y directions, respectively.

The electric field vector $\boldsymbol{E}^{(2)}$ which has passed the modulator Mo can be written as

$$\boldsymbol{E}^{(2)}=\frac{E}{\sqrt{2}}\boldsymbol{i}+\frac{E}{\sqrt{2}}\mathrm{e}^{\mathrm{i}\delta}\boldsymbol{j}, \qquad (A\cdot 2)$$

where δ is represented by eq. (1).

Since the reflection by the sample S is defined in terms of the Fresnel reflection coefficients $\hat{r}_{\pm}$ for RCP and LCP, we can rewrite eq. (A·2) using the unit vectors for circular polarizations, $\boldsymbol{r}$ and $\boldsymbol{l}$, defined by

$$\boldsymbol{r}\equiv(\boldsymbol{i}+\mathrm{i}\boldsymbol{j})/\sqrt{2}, \quad \boldsymbol{l}\equiv(\boldsymbol{i}-\mathrm{i}\boldsymbol{j})/\sqrt{2}. \qquad (A\cdot 3)$$

Then we obtain

$$\boldsymbol{E}^{(2)}=\frac{E}{2}\{(1-\mathrm{i}\,\mathrm{e}^{\mathrm{i}\delta})\boldsymbol{r}+(1+\mathrm{i}\,\mathrm{e}^{\mathrm{i}\delta})\boldsymbol{l}\}. \qquad (A\cdot 4)$$

By using the Fresnel coefficients $\hat{r}_{\pm}$ we have for the electric field vector $\boldsymbol{E}^{(3)}$ of the reflected light,

$$\boldsymbol{E}^{(3)}=\frac{E}{2}\{(1-\mathrm{i}\,\mathrm{e}^{\mathrm{i}\delta})\hat{r}_{+}\boldsymbol{r}+(1+\mathrm{i}\,\mathrm{e}^{\mathrm{i}\delta})\hat{r}_{-}\boldsymbol{l}\}. \qquad (A\cdot 5)$$

By replacing $\boldsymbol{r}$ and $\boldsymbol{l}$ by $\boldsymbol{i}$ and $\boldsymbol{j}$ using eq. (A·3), we get for $\boldsymbol{E}^{(3)}$

$$\begin{aligned}\boldsymbol{E}^{(3)}=&\frac{E}{2\sqrt{2}}\{(\hat{r}_{+}+\hat{r}_{-})-\mathrm{i}\,\mathrm{e}^{\mathrm{i}\delta}(\hat{r}_{+}-\hat{r}_{-})\}\boldsymbol{i}\\&+\frac{E}{2\sqrt{2}}\{(\hat{r}_{+}-\hat{r}_{-})+\mathrm{i}\,\mathrm{e}^{\mathrm{i}\delta}(\hat{r}_{+}+\hat{r}_{-})\}\boldsymbol{j}.\end{aligned} \qquad (A\cdot 6)$$

The amplitude of the electric field vector which is transmitted through the analyzer A is given by the x'-component of $\boldsymbol{E}^{(3)}$ and can be expressed as

$$\begin{aligned}E_{x'}&=E_{x}^{(3)}\cos\phi+E_{y}^{(3)}\sin\phi\\&=\frac{E}{2\sqrt{2}}\{\hat{r}_{+}(1-\mathrm{i}\,\mathrm{e}^{\mathrm{i}\delta})\,\mathrm{e}^{\mathrm{i}\phi}+\hat{r}_{-}(1+\mathrm{i}\,\mathrm{e}^{\mathrm{i}\delta})\,\mathrm{e}^{-\mathrm{i}\phi}\}.\end{aligned} \qquad (A\cdot 7)$$

Thus eq. (2) has been derived.

References

1) C. C. Robinson: J. Opt. Soc. Am. **53** (1963) 681.
2) J. C. Suits: Rev. Sci. Instrum. **42** (1971) 19.
3) S. N. Jasperson and S. E. Schnatterly: Rev. Sci. Instrum. **40** (1969) 761.
4) G. A. Osborne, J. C. Cheng and P. J. Stephens: Rev. Sci. Instrum. **44** (1973) 10.
5) R. A. Shatwell and A. J. McCaffery: Phys. Rev. **B12** (1975) 3815.
6) K. Sato: J. Phys. Soc. Jpn. **43** (1977) 719.
7) P. Chaudhari, J. J. Cuomo and R. J. Gambino: Appl. Phys. Lett. **22** (1973) 337.
8) S. Visnovski, B. Knappe, V. Prosser and H. R. Muller: Phys. Status Solidi (a) **38** (1976) K53.
9) A. P. Malozemoff, J. P. Jamet and R. J. Gambino: *Proc. Intermagnetic Conf.*, IEEE Trans. Magn. **MAG13** (1977) 1609.